J. Fluid Mech. (1979), *vol.* 94, *part* 4, *pp.* 745–775
Printed in Great Britain

Local isotropy and large structures in a heated turbulent jet

By K. R. SREENIVASAN,
Department of Mechanics and Materials Science, The Johns Hopkins University, Baltimore, Maryland 21218

R. A. ANTONIA AND D. BRITZ†
Department of Mechanical Engineering, University of Newcastle, New South Wales, 2308

(Received 13 July 1978 and in revised form 9 February 1979)

Recent measurements of the skewness of the derivative of the temperature fluctuation θ, implying the breakdown of local isotropy even in high Reynolds number shear flows, are examined. Using the temperature signal in a slightly heated axisymmetric jet, a detailed quantitative analysis is made of the suggestion that the observed presence of a well-defined large-scale pattern of the temperature signal in these flows is responsible for this breakdown. A selective ensemble averaging technique is used for separating this pattern from fluctuations superposed on it. The technique is extended to extract the large-scale patterns in simultaneously measured axial (u), radial (v) velocity fluctuations, and the products uv, $u\theta$ and $v\theta$, so that it is possible to separate contributions of these patterns from those of the superposed fluctuations to several important turbulent quantities. The mean shape of the patterns, their degree of anisotropy and correlation, and their contribution to turbulence intensities and Reynolds shear stress are obtained. Probability densities and spectra of these quasi-homogeneous superposed fluctuations are also obtained. Results show that the fluctuations are consistent with local isotropy and make the dominant contribution to the turbulence intensities, that the large-scale patterns are responsible for the observed skewness values of the derivative of v, and that the fluctuations may be responsible for a significant part of the turbulent momentum and heat transport, especially in the region of the jet where the turbulent energy production is substantial.

1. Introduction

The concept of local isotropy is of central importance to the theory of turbulence because its validity implies a certain universality of the small-scale motion. Local isotropy (or isotropy at small scales) implies that the small-scale structure becomes independent of details of any orientation effects introduced by the mean shear. Several implications of local isotropy have been verified by many earlier experiments (e.g. Corrsin 1949; Townsend 1948). Recently, however, as more and more detailed

† Present address: Kemisk Institut, Aarhus Universitet, 8000 Aarhus, Denmark.

0022–1120/79/4306–7560 $02.00

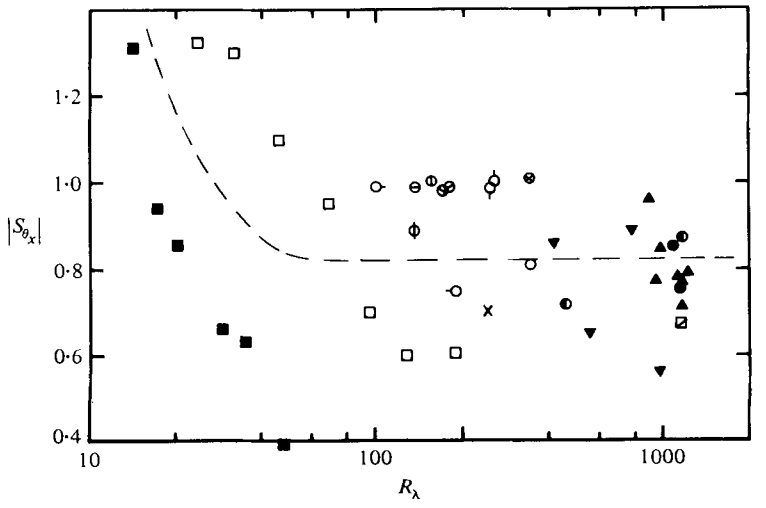

FIGURE 1. Variation of $|S_{\theta_x}|$ with R_λ. Gibson *et al.* (1977): ○, atmospheric boundary layer; ◐, heated jet; ●, heated wake; ⊘, cooled wake, ▲, Mestayer *et al.* (1976), heated boundary layer. ▼, Gibson *et al.* (1970), atmospheric boundary layer (corrected for velocity sensitivity); ×, Antonia & Van Atta (1975), heated jet. Freymuth & Uberoi (1971, 1973): □, heated two-dimensional wake; ■, heated axisymmetric wake. ⊖, ⓘ, ⊘, ⊘, Sreenivasan, Antonia & Danh (1977), heated boundary layer. ◪, our unpublished data, atmospheric surface layer. ⊖, ⊖, ⊖, ⊖, ⊖, present data, axisymmetric heated jet, η = 0, 0·89, 1·15, 1·48 and 1·63 respectively. ———, suggested mean trend.

parameters are measured with increasingly reliable and sophisticated instrumentation, experimental evidence in apparent conflict with local isotropy of shear flow turbulence appears to be accumulating. Perhaps the most significant evidence is the observation, in both laboratory and atmospheric flows, that the skewness S_{θ_x} of the streamwise derivative θ_x is a non-zero quantity of magnitude about 1. (The other relevant evidence is discussed by Sreenivasan, Antonia & Britz 1978.) The skewness data obtained by various authors in several flows are summarized in figure 1. The data cover a fairly wide range of the microscale Reynolds number† R_λ ($\equiv u'\lambda/\nu$, where u' is the root-mean-square fluctuation of the streamwise velocity, λ is the Taylor microscale and ν is the kinematic viscosity). In spite of the considerable scatter, it is clear that $|S_{\theta_x}|$ exhibits no significant trend with R_λ for $R_\lambda \gtrsim 50$; the mean value is about 0·8.

If the Reynolds number is sufficiently large, it seems logical to expect local isotropy to prevail at all wavenumbers which contribute most to θ_x. Detailed calculations (see appendix A) show that this is indeed to be expected even at moderate Reynolds numbers, say R_λ of about 100. It then follows from reflexional symmetry that an odd order mean value such as $\overline{\theta_x^3}$ should be zero in most of the flows represented in figure 1. The evidence in figure 1 has therefore been regarded as a direct violation of

† Strictly speaking, the relevant parameter here must be the Péclét number $u'\lambda_\theta/k$ where λ_θ is the temperature microscale and k is the thermal diffusivity. But the ratio of Péclét to Reynolds numbers is a constant of order 1 in these flows, so that it is convenient and sufficiently precise to use Reynolds number as the only relevant parameter.

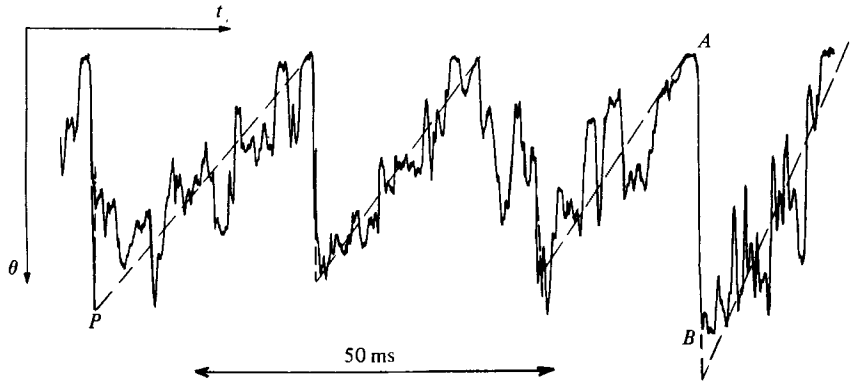

FIGURE 2. Presence of ramps in a trace of temperature in axisymmetric heated jet, obtained in the region of maximum production of turbulent energy. Intermittency factor $\simeq$ 0·93.

local isotropy. Wyngaard (1971) attempted to explain this paradoxical result by the possibility of the contamination of the measured temperature by the velocity sensitivity of the temperature wire. The error due to this velocity contamination is now known to be much smaller (at least in the more recent measurements) than that anticipated by Wyngaard (see, e.g., Gibson, Friehe & McConnell 1977; Mestayer *et al.* 1976); further this correction is always positive while the measured skewness may be of either sign. (Gibson *et al.* (1977) find that the sign of S_{θ_x} is the same as that of the product of the mean vorticity and the mean temperature gradient.)

A possible alternative explanation (Gibson *et al.* 1977; Sreenivasan & Antonia 1977) is that the apparent breakdown of local isotropy relates to the presence of certain well-defined patterns in turbulent signals even for high Reynolds number shear flows. For example, it is well recognized (see, e.g., Antonia, Prabhu & Stephenson 1975; Mestayer *et al.* 1976; Gibson *et al.* 1977) that the temperature signals exhibit certain ramp-like patterns, both at moderate and high Reynolds numbers. Figure 2 shows a trace of temperature fluctuation in an axisymmetric jet; the ramps are also indicated tentatively in the figure. These ramp-like patterns may not be as clearly defined at all points in the flow, but the trace of figure 2 is in fact typical of temperature fluctuations in the region of maximum production of turbulent energy. (There is inevitably some ambiguity in the exact definition of the ramp, but this is considered in some detail in § 3.) The presence of sharp edges (such as AB in figure 2) in the ramps suggests that a part (though small) of the high frequency content of θ arises directly from the ramps. Because of the asymmetry of the ramps, this small fraction of the derivative θ_x is definitely skewed; this, we believe, is important. In fact, preliminary calculations (Sreenivasan & Antonia 1977) have shown that the part of θ_x responsible for the observed non-zero magnitude of S_{θ_x} arises almost exclusively from these ramps and not from the small scale.

The temperature trace shown in figure 2 is for a radial position in the jet where, on average, the flow is turbulent for about 93% of the time. Further out into the intermittent region, the excursions (i.e. parts of the signal whose amplitude exceeds a certain pre-set threshold value) in the temperature signal are not as ramp-like as shown in figure 2 but, as we shall show in §§ 3 and 4, they too possess, on average, a

skewed derivative, so that the argument of the previous paragraph is relevant also to strongly intermittent turbulent signals.

The original motivation of the present work was to examine, on a quantitative basis, the relation between these patterns and observations suggesting the breakdown of local isotropy. We proceeded to do this by extracting patterns from the temperature signal and evaluating their contribution to the skewness of θ_x. As it soon became clear that a simple extension of the technique would allow us to evaluate separately contributions of similar patterns in other turbulent signals from those of the superposed turbulence to any flow property, such as the turbulent energy or the Reynolds shear stress, we addressed ourselves to this general problem.

The possible physical significance of splitting a turbulent signal into a more or less well-defined pattern and superposed fluctuations is worth examining. The length scale associated with the ramp-like pattern is comparable in magnitude to the mean flow width, and the magnitude of the temperature rise in a ramp (e.g. AB in figure 2) is comparable to the total variation of the temperature in the flow. It seems therefore reasonable to interpret the ramp as the signature of the large-scale structure in a turbulent shear flow. Although caution is required (as discussed in § 4 *c*) because of the three-dimensionality of the large structure and the inherent limitations of single probe measurements, the present study may help to assess the possible importance of the large structure to the dynamics of the flow. It is also worth emphasising that the superposed turbulence is not simply the small-scale dissipative turbulence, although it includes dissipative scales. In fact, it is shown in § 4 that the superposed turbulence contains most of the energy, and is hence somewhat identifiable with Townsend's (1976, p. 107) 'main turbulent motion'. We share Townsend's concern that a clear distinction may not be drawn between a 'main turbulent motion' and a set of 'large eddies', but, as in Townsend's case, we find it convenient to discuss the turbulent motion as if the distinction were valid.

In § 2, we discuss details of the technique by which different features of the large scale patterns and superposed turbulence are separated; this section also contains details of experimental conditions and instrumentation. In § 3, we present average shapes of the large-scale patterns in u, v, θ, uv, $u\theta$, and $v\theta$ signals. Statistical properties of the superposed turbulence are examined in some detail in § 4, with special emphasis on local isotropy. These results are discussed in § 5. A simple assessment of conventional requirements of local isotropy is made for the present flow in appendix A. Appendix B is a critical examination of the technique used for generating information about the large structure or, more precisely, its signature.

2. Experimental conditions and technique

2.1. *The jet*

The jet used for this study was supplied by a laboratory high pressure air supply at a constant velocity at the nozzle exit (diameter $\simeq$ 2 cm) of 32 m s^{-1}. The air supply was heated electrically to a temperature of 34 °C above ambient. The jet Reynolds number at the exit was $2{\cdot}8 \times 10^4$. The jet exhausted into a co-flowing external stream at a constant speed and constant temperature, supplied by a centrifugal blower. All measurements were made at a single streamwise station 59 diameters downstream

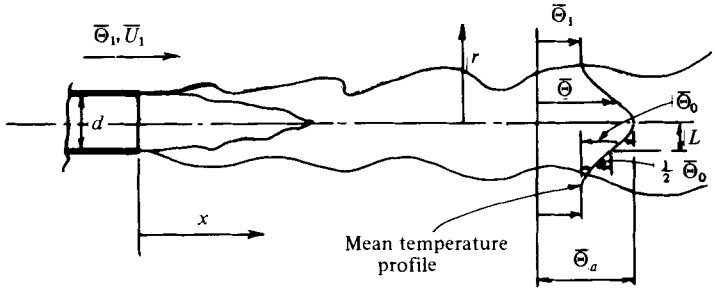

FIGURE 3. Sketch defining notation.

of the nozzle exit. Figure 3 shows a schematic diagram and defines the co-ordinate axes. L denotes the radial distance from the jet axis to the position corresponding to half the maximum temperature (above ambient). The co-ordinate η is defined as the ratio r/L.

2.2. *Notation*

U and V are the components of instantaneous velocity in the streamwise direction x and radial direction r respectively; Θ is the instantaneous temperature. Each variable X (where X denotes U, V or Θ) can be split into its (time) mean value $\bar{X}$, defined by

$$\bar{X} = \lim_{\tau\to\infty} \tau^{-1} \int_0^\tau X(t)\, dt,$$

and the fluctuating part x; here τ is time. By definition, $\bar{x} = 0$. If, at the point of measurement, the flow is intermittently turbulent, conditional averages $\bar{X}_t$ are defined (over the turbulent part of the flow only) by the relation $\bar{X}_t = \overline{IX}/\bar{I}$, where the intermittency function I is equal to one or zero, depending upon whether the flow is turbulent or not. $\bar{I} = \gamma$ is the intermittency factor.

Suffixes 1 and a are used to denote conditions corresponding to free-stream and jet axis respectively; suffix 0 denotes values at the jet axis in excess of free-stream values: $\bar{X}_a = \bar{X}_1 + \bar{X}_0$. At the measuring station, $L = 6{\cdot}5$ cm, $\bar{U}_0 = 3{\cdot}1$ m s^{-1}, $\bar{\Theta}_0 = 3{\cdot}3$ °C, $\bar{U}_1 = 4{\cdot}85$ m s^{-1}, $\bar{\Theta}_1 = 15$ °C.

2.3. *Measurement and processing*

Velocity fluctuations u and v were obtained with a platinum-coated tungsten X-probe (5 μm diameter wires) operated with two DISA 55M01 constant temperature anemometers. The temperature fluctuation θ was measured with a 1 μm diameter Wollaston wire located approximately 1 mm below the mid-point of the X-probe. The temperature wire was operated at a constant current of 0·1 mA, which is low enough to ensure negligible velocity sensitivity. Hot-wire signals were decontaminated for their sensitivity to temperature, in the manner described by Antonia *et al.* (1975). Signals proportional to (decontaminated) u and v, and θ were recorded simultaneously on a Philips ANALOG-7 FM tape recorder whose upper frequency response at the speed of recording was flat up to 5 kHz. The recorded signals were later played back into an A/D converter (10 bit including sign) and the digitized signals stored on magnetic tapes which were then processed on an ICL 1904 computer. The sampling frequency used was 12 kHz (real time). Most records had a (real time) duration of 27·7 s. For a few runs, a record duration of 70·4 s was used.

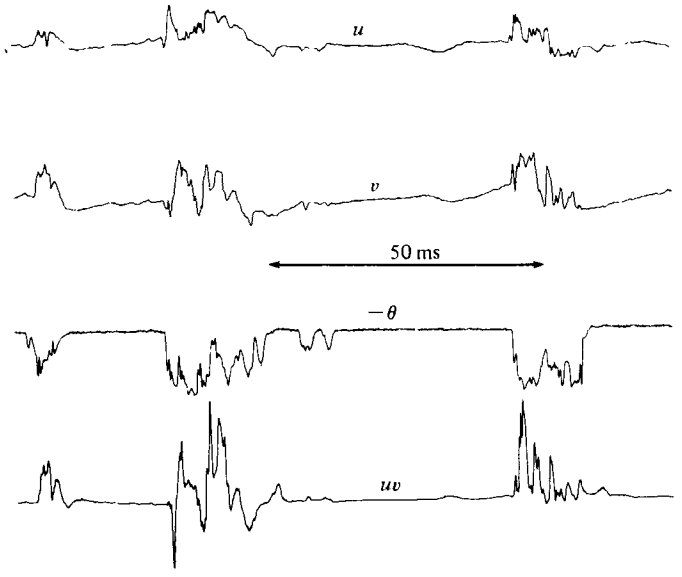

FIGURE 4. Simultaneous records of u, v, θ and uv at an intermittent radial position, $\eta = 1{\cdot}48$ ($\gamma \simeq 0{\cdot}28$).

2.4. *Technique for separating contributions from the large-scale and superposed tubulence*

The mean shape of excursions was obtained by ensemble averaging. As excursions have a wide range of duration, it is clear that ensemble averaging over excursions of all durations will smear the resulting mean shape. In order to avoid this, it is ideally necessary to restrict members of the ensemble to a given duration. However, practical considerations dictate that a small, but finite, range of durations be used. We recall that Antonia & Atkinson (1976) have determined that ramps of a given duration do not have widely varying peak amplitudes. This means that, by restricting ourselves to a narrow range of duration, we also consider a narrow range of peak amplitudes, thus ensuring the general similarity of shape for different members of the ensemble. This not only makes all ensemble average operations more meaningful than they would otherwise be, but also ensures a fairly rapid convergence. Ideally, of course, the finite range of duration must be as small as possible. Different mean durations as well as different ranges of duration around the mean value were tried, and the effects determined (see § 3).

Identification and definition of duration of excursions is usually more precise with temperature than with velocity signals. The duration T of an excursion is defined as the time interval between an upcrossing and a subsequent downcrossing of a certain pre-set threshold. If heat acts as a passive scalar, it is highly plausible that the momentum and thermal interfaces will be identical, provided that the momentum and thermal flows have a common origin. In such cases, intermittency functions generated either from temperature or velocity fluctuations have led essentially to the same intermittency distributions (Sunyach & Mathieu 1969; Jenkins & Goldschmidt 1976). A more direct indication of the accuracy of this assumption is provided in figure 4, which shows simultaneously measured traces of u, v and θ and

the product uv at an intermittent flow position, $\eta = 1{\cdot}48$ ($\gamma \simeq 0{\cdot}28$). The figure also shows that the small separation of the velocity and temperature wires was not too crucial for these considerations. So it is clear that, whenever θ is turbulent, u and v are too. This is true of the products uv (shown in figure 4) and $u\theta$ and $v\theta$ (not shown). Thus, ensemble averaging operations on u and v and products uv, $u\theta$ and $v\theta$ are performed over those parts which coincide in time with the occurrence of an excursion in θ. The ensemble averaging technique itself consists of the following steps. The time interval between two successive points, at which the temperature exceeds, during an upcrossing, and falls below, during the subsequent downcrossing, the pre-set threshold level is determined first. (The effect of changing the threshold level will be discussed in § 3.) Then, if the duration between these two points lies within the range of interest, amplitude levels of u, v or θ, and uv, $u\theta$ or $v\theta$ are obtained, by interpolation if necessary, at S equally spaced points within the excursion. (For convenience, S was chosen as the ratio of the mean duration to the sampling interval.) A subsequent excursion in the same range of duration is treated similarly, and the amplitudes at the S points are added to the previous set of values at corresponding locations. Ensemble-averaged shapes, denoted by $\langle\ \rangle$, are obtained by dividing the sum at each of the S points by the total number N of excursions belonging to the chosen range of duration. For convenience, we shall henceforth use the expression 'given duration $\overline{T}$' to signify 'given range of duration centred about $\overline{T}$', where $\overline{T}$ denotes the arithmetic mean of the extreme values of the chosen range.

The mean value of the ensemble average is defined by

$$\langle\overline{\overline{X}}\rangle = \frac{1}{\overline{T}}\int_0^{\overline{T}} \langle X\rangle\, dt, \tag{2.1}$$

where t ($0 \leqslant t \leqslant \overline{T}$) is the running time within the excursion (or the ensemble average of excursions). The double bar here and elsewhere indicates the time average over the duration corresponding to the ensemble of large-scale excursions. The quantity obtained by subtracting $\langle X\rangle$ from the ith member X_i of the ensemble represents the superposed motion $x_{s,i}$, viz.

$$x_{s,i} = X_i - \langle X\rangle. \tag{2.2}$$

It is clear that $x_{s,i}$ also form an ensemble with the same number of members as the original ensemble. The total superposed motion x_s is made up of the collection of $x_{s,i}$, over all the members of the ensemble. By definition, $\langle x_s\rangle \equiv 0$, where the ensemble average is taken, as previously, over members $x_{s,i}(\overline{T})$ of the ensemble. It is also clear that $\overline{\overline{x}}_s = 0$. Further if $\overline{T}$ is large enough to yield a steady time average of superposed fluctuations, $\overline{\overline{x}}_{s,i} \simeq 0$ for each member i of the ensemble. This further means that, for large $\overline{T}$,

$$\langle\overline{\overline{X}}\rangle \simeq \overline{X}_t. \tag{2.3}$$

We can also define the 'r.m.s.' of x_s by the relation

$$x_s''^2 \equiv \langle\overline{\overline{x_s^2}}\rangle = \frac{1}{\overline{T}}\int_0^{\overline{T}} \langle x_s^2(t)\rangle\, dt, \quad 0 \leqslant t \leqslant \overline{T}, \tag{2.4}$$

$$= \overline{\overline{\langle (X - \langle X\rangle)^2\rangle}}.$$

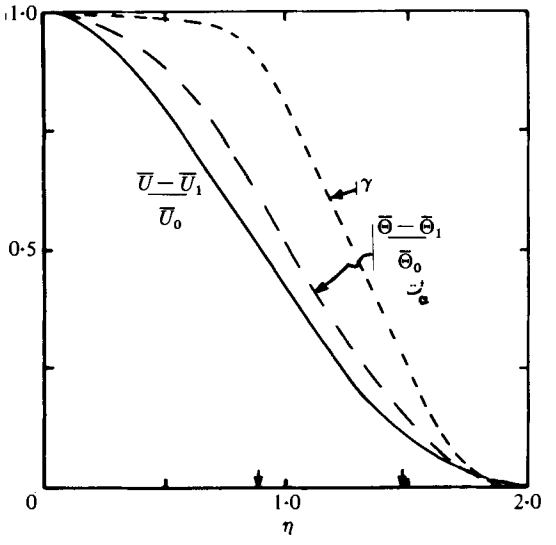

FIGURE 5. Mean velocity, mean temperature and intermittency profiles across the jet. ↓ on the abscissa show the two radial positions (η = 0·89 and 1·48) at which most of the data is presented here.

Because ensemble averaging is performed over excursions in a given range of duration, the superposed motion defined by (2.4) is also defined over the same duration $\overline{T}$ and is, where necessary, referred to as $x_s(\overline{T})$. Obviously, (2.4) defines only a subset of the totality of the superposed motion. This totality of the superposed motion is the collection of $x_{s,i}$ evaluated over the entire range of large-scale excursions. However, we shall show in § 4 that a properly chosen subset is a good representative of the totality.

Probability density functions of the superposed turbulence were obtained in the usual manner by counting the number of digital points at a given level of x_s and dividing them by the total number and the window width of the digital levels. The probability densities of the derivatives were obtained by differentiating each of the $x_{s,i}$ and treating this as another independent signal.

The power spectral density of the superposed turbulence was also obtained. By definition, this requires that the spectral density be computed over the ensemble of $x_{s,i}$, but here this is approximated by stringing the ensemble members $x_{s,i}$ together and using a fast Fourier algorithm on this collection. Treating this collection as a continuous entity poses no special problems, because only frequencies comparable to the sampling frequency can be expected to be affected by this artifice.

3. Results: ensemble average shapes

For reference purposes, mean (axial) velocity, mean temperature and intermittency profiles across the jet are given in figure 5. Other mean and turbulent quantities have been given in Antonia *et al.* (1975).

Figure 6 shows ensemble averages of temperature excursions of different durations. From the examples shown, it appears that, for durations somewhat smaller than the characteristic mean flow time $L/\overline{U}_a$, the ensemble average shapes are symmetrical.

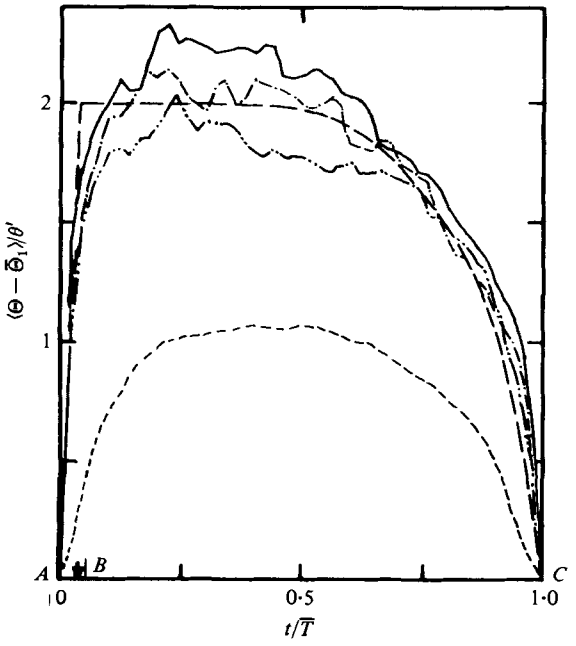

FIGURE 6. Ensemble average distributions of excursions of various durations in the temperature signal, $\eta = 0{\cdot}89$: ---, $\bar{T}\bar{U}_a/L = 0{\cdot}38$, $\Delta\bar{T}/\bar{T} = \pm 0{\cdot}5$, $N = 194$; —··—, 1·12, ±0·11, 84; —·—, 1·63, ±0·08, 66; ——, 2·25, ±0·11, 112.

It follows that they do not, on average, contribute to the skewness of θ_x. On the other hand, ensemble averages of large duration excursions have well-defined asymmetrical shapes. Clearly, their contribution to $\overline{\theta_x^3}$ is significant (e.g. Sreenivasan & Antonia 1977; Freymuth 1978).† Also, as ensemble average shapes for $\bar{T} \gtrsim L/\bar{U}_a$ are very nearly similar, it seems sufficient, in future, to restrict our attention to durations of this type.

Similarly, although not shown here, ensemble averages of excursions of v (and of u) of duration smaller than $L/\bar{U}_a$ are very nearly symmetrical, and contribute nothing to the skewness of the derivative v_x (and of u_x). It is worth mentioning that they are almost exactly like ensemble averages of pseudo-bulges of white noise generated by setting an arbitrary artificial threshold (see appendix B). Again, for $\bar{T} \gtrsim L/\bar{U}_a$, the shapes of ensemble averages are essentially independent of $\bar{T}$, so that only one representative set needs to be discussed.

As typical examples of average shapes of large-scale excursions, figures 7(*a*)–(*f*) show results (for four values of η) of computations described in § 2.4, for excursions of mean duration $\bar{T}\bar{U}_a/L = 2{\cdot}5$. The interval $\Delta\bar{T}$ used for selecting members of the ensemble is $\pm 0{\cdot}2\bar{T}$. In these plots, five neighbouring points were averaged arithmetically. In figures 7(*a*)–(*c*), results are presented in the form $(\langle X\rangle - \bar{X}_1)/\bar{X}_0$ *vs.* $t/\bar{T}$,

† The asymmetrical temperature shape can be characterized by two length scales. The length associated with the gradual fall in temperature may be taken proportional to the integral length scale of the flow. The length characteristic of the steeper slope is more likely to be associated with the small scale of the turbulence. Freymuth (1978) has shown that, for a linear-ramp model, if this latter scale is proportional to the Kolmogorov scale, the ramp model is consistent with the result that S_{θ_x} is independent of R_λ.

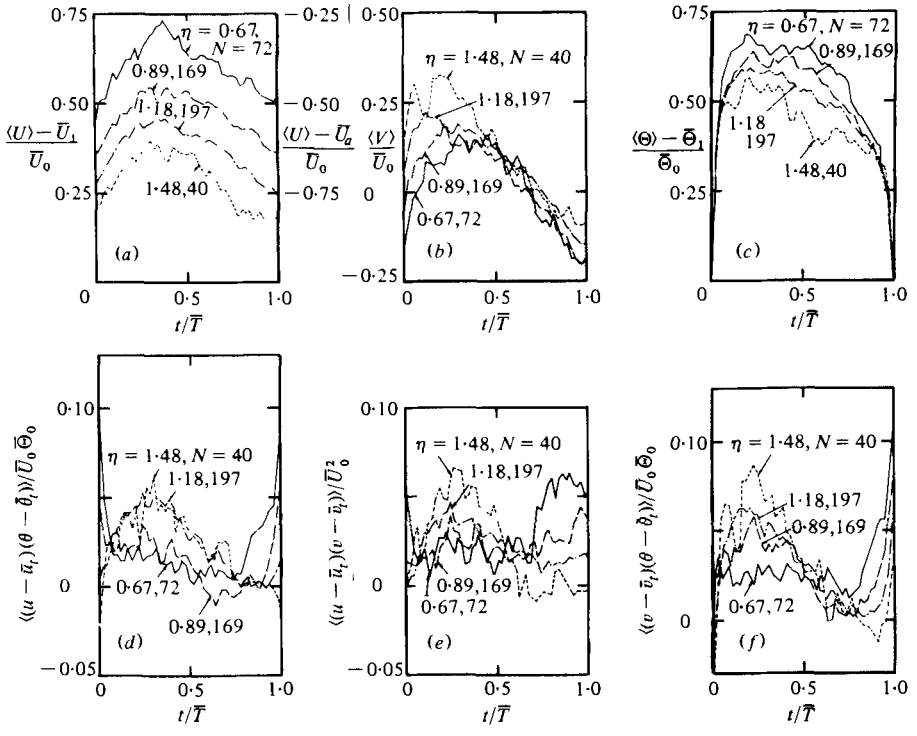

FIGURE 7. Ensemble-averaged distributions of U, V, Θ and of their products in bulges of duration $\bar{T} = 2{\cdot}5L/\bar{U}_a$; $\Delta\bar{T}/\bar{T} = \pm 0{\cdot}2$. ($N$ refers to the number of bulges found at the particular value of η.)

where the time t is measured from the leading or downstream edge of an excursion. There are several possible ways of plotting the results, but this form was suggested by the conventional use of $(\bar{X}-\bar{X}_1)/\bar{X}_0$ *vs.* η when self-preservation of the quantity $\bar{X}$ is considered. Clearly, $(\langle X\rangle-\bar{X})/\bar{X}_0$ or $(\langle X\rangle-\bar{X}_t)/\bar{X}_0$ would have been as interesting, as considerations described in appendix B would suggest, but such quantities can be obtained from the present data by simple linear transformations. Figure 7(*a*) shows that interface bulges of a given duration have the largest axial velocity closest to the axis. When referred to the local mean velocity $\bar{U}$ (or the conditional mean turbulent velocity $\bar{U}_t$), however, ensemble averages $(\langle U\rangle-\bar{U}_1)/\bar{U}_0$ [or $(\langle U\rangle-\bar{U}_t)/\bar{U}_0$] are smaller near the axis (see the ordinate scale on the right side of figure 7*a*). This result is consistent with the notion that bursts of high-momentum fluid occur away from the jet axis (Sreenivasan & Antonia 1978). In general, $\langle U\rangle$ shapes are nearly symmetrical. In contrast, $\langle V\rangle$ shapes have relatively sharp fronts and gradually sloping backs. This last feature is even more pronounced for $\langle\Theta\rangle$, and is in qualitative agreement with LaRue & Libby's (1976) ensemble averages of θ in a turbulent wake. There is a significant region near the backs where $\langle V\rangle$ is negative, and essentially independent of η, at least for the range of η covered in the experiment. These results show that while the outward motion may be stronger at larger η, the entrainment that occurs on the backs of interface bulges is essentially independent of η. The maximum value of $\langle\Theta\rangle-\bar{\Theta}_1$, decreases somewhat with increasing η (in contrast to $\langle V\rangle$), although retaining essentially the same sharp leading edges. It is

interesting to note that the ensemble averages of Θ are substantially different from the somewhat simplified ramps suggested in § 1 (see figure 2), and are closer to the exponential 'ramps' examined by Antonia & Atkinson (1976). However, as indicated in § 2.4, it is clear from figures 7 (*b*) and (*c*) that the large-scale excursions do contribute to the skewness of the respective derivatives through their sharp leading edges and the comparatively gradually sloped trailing edges. Quantitative estimates of this effect are given in § 4.

Figure 8 (*a*)–(*f*) shows the effect of varying $\Delta\overline{T}$ for a given $\overline{T}$ on the ensemble average calculations at $\eta = 0{\cdot}89$. Here, $\overline{T}\overline{U}_a/L = 2{\cdot}5$ and $\Delta\overline{T}/\overline{T}$ varies by nearly a factor of 2·5. It is clear that the actual choice of $\Delta\overline{T}$ in this range is not a critical factor for obtaining the essential features of the ensemble average shapes. Also shown in figure 8 are the 95% confidence intervals for the case $\Delta\overline{T}/\overline{T} = \pm 0{\cdot}2$. Results shown in figure 8 correspond to a threshold which is different from that used for obtaining data of figure 7, the difference being approximately equal to the uncertainty in determining the proper threshold. A quick comparison between figure 7 (*a*)–(*c*) and 8 (*a*)–(*c*) shows that the threshold setting is not critical. The confidence intervals in figure 8 (*d*)–(*f*) show that the reliability of the ensemble averages of products is, as expected, poorer than that of individual quantities; they also show that the effect of jitter (i.e. the precise choice of $\Delta\overline{T}$) is more pronounced. Even so, two properties stand out clearly (see figure 7 *d*–*f*). First, $\langle uv\rangle$, $\langle u\theta\rangle$ and $\langle v\theta\rangle$ are all positive almost throughout the duration of the large-scale excursions. As $\overline{uv}$, $\overline{u\theta}$ and $\overline{v\theta}$ are all positive in a jet, it is clear that the contribution to turbulent transport of the ensemble-averaged large-scale excursions is positive nearly everywhere. We also note that the products $\langle u\rangle\langle v\rangle$, $\langle u\rangle\langle\theta\rangle$ and $\langle v\rangle\langle\theta\rangle$ are also nearly always positive, suggesting a high degree of positive correlation between any pair of ensemble-averaged large-scale excursions. Quantitative estimates of this correlation are given in § 4 (*c*). Second, with increasing η, a gradual change occurs in the ensemble average shapes. Close to the region of maximum turbulent energy production ($\eta = 0{\cdot}67$ for example), a large fraction of the contribution to the average shear stress or heat flux occurs close to the back of the excursion ($t/\overline{T} \gtrsim 0{\cdot}7$); a small region where this contribution is relatively large can also be identified quite close to the front ($t/\overline{T} \lesssim 0{\cdot}1$), especially in $\langle uv\rangle$ and $\langle v\theta\rangle$. As η increases, no significant contribution to $\langle\overline{\overline{uv}}\rangle$, $\langle\overline{\overline{u\theta}}\rangle$ or $\langle\overline{\overline{v\theta}}\rangle$ arises from the immediate vicinity of the front or the back; instead, most of the contribution is provided by regions well within the excursions. For example, at $\eta = 1{\cdot}48$, this region is $0{\cdot}1 \lesssim t/\overline{T} \lesssim 0{\cdot}6$.

4. Statistics of superposed turbulence

(*a*) *Mean-square values*

In this section, we examine the properties of the superposed motion, as defined in § 2.4. In particular, we examine whether it is consistent with the requirements of local isotropy. In doing so, we should first establish that properties of this superposed motion are independent of the duration $\overline{T}$ for which it is defined (see § 2.4). Figures 9 (*a*) and (*b*) show normalized r.m.s. values of small-scale u and v, namely $u_s''/\overline{U}_0$ and $v_s''/\overline{U}_0$, plotted as a function of the duration $\overline{T}$, for $\eta = 0{\cdot}67$, 0·89 and 1·48. Figure 9 (*c*) shows a similar plot of $\theta_s''/\overline{\Theta}_0$. Although these r.m.s. values show a

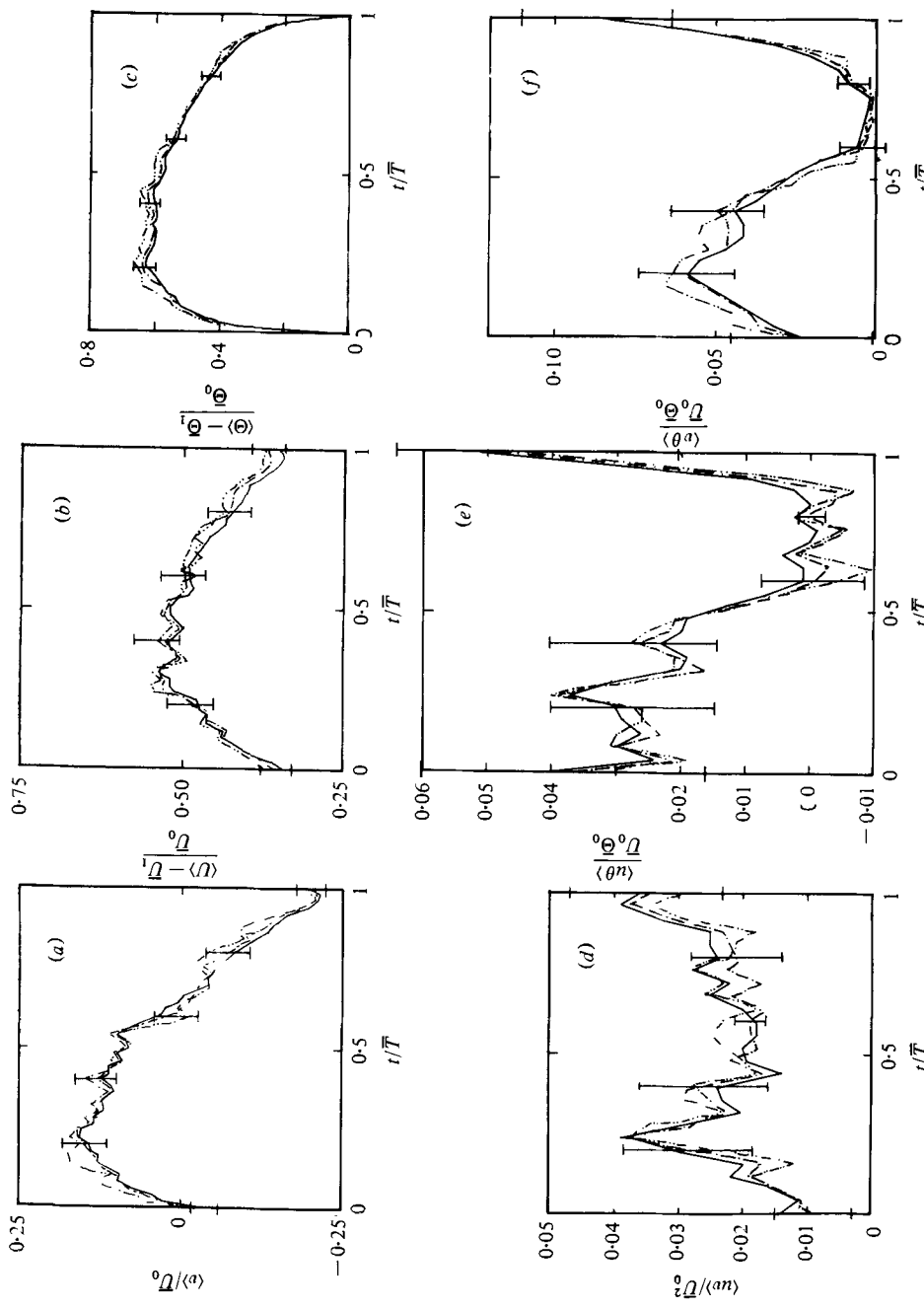

FIGURE 8. Effect of varying range of duration $\Delta\bar{T}/\bar{T}$ on the ensemble average distributions. $\eta = 0{\cdot}89$. ——, $\Delta\bar{T}/\bar{T} = \pm 0{\cdot}28$; – – –, $\pm 0{\cdot}2$; –·–·–, $\pm 0{\cdot}12$. Vertical bars indicate 95 % confidence intervals for $\Delta\bar{T}/\bar{T} = \pm 0{\cdot}2$.

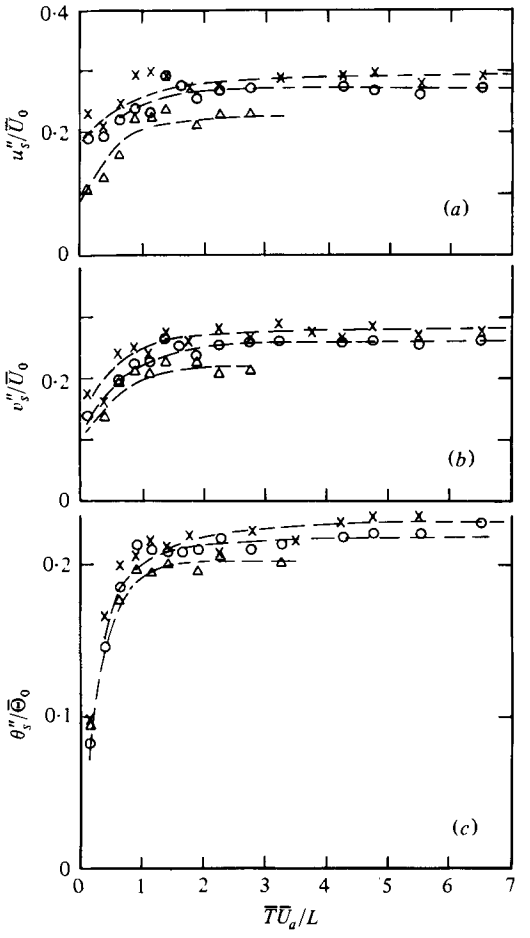

FIGURE 9. Variation of the 'r.m.s.' values of u_s, v_s and θ_s as a function of $\bar{T}$. Broken lines are drawn through the points for clarity. ×, η = 0·67; ○, 0·89; △, 1·48. (*a*) $u_s''/\bar{U}_0$; (*b*) $v_s''/\bar{U}_0$; (*c*) $\theta_s''/\bar{\Theta}_0$.

dependence on $\bar{T}$ for $\bar{T}\bar{U}_a/L \lesssim 1$, they are very nearly independent of $\bar{T}$ for $\bar{T}\bar{U}_a/L \gtrsim 1$. This near independence of $\bar{T}$ provides some *a posteriori* justification for the selection of a subset (in the region $\bar{T}U_a/L \gtrsim 1$), rather than the totality of the superposed motion (see § 2.4). Ideally, we must show that this behaviour is true of higher moments as well, but we soon run into convergence problems because of the limitation on the length of data records. A possible, although speculative, explanation for the dependence of $u_s''/\bar{U}_0$, $v_s''/\bar{U}_0$ and $\theta_s''/\bar{\Theta}_0$ on $\bar{T}$ for $\bar{T} \lesssim L/\bar{U}_a$ is as follows. It seems likely that small excursions, in Θ for example, occur largely when either top edges or sides of the large-scale structures skim past the sensor. A large fraction of these small excursions is presumably related to the viscosity-dependent superlayer. The relative fraction of this viscosity dependence should decrease in magnitude with increasing $\bar{T}$ and, at sufficiently large $\bar{T}$, should be of little consequence. Empirically, the range $\bar{T} \gtrsim L/\bar{U}_a$ appears to be sufficiently large for asymptotic values of $u_s''/\bar{U}_0$,

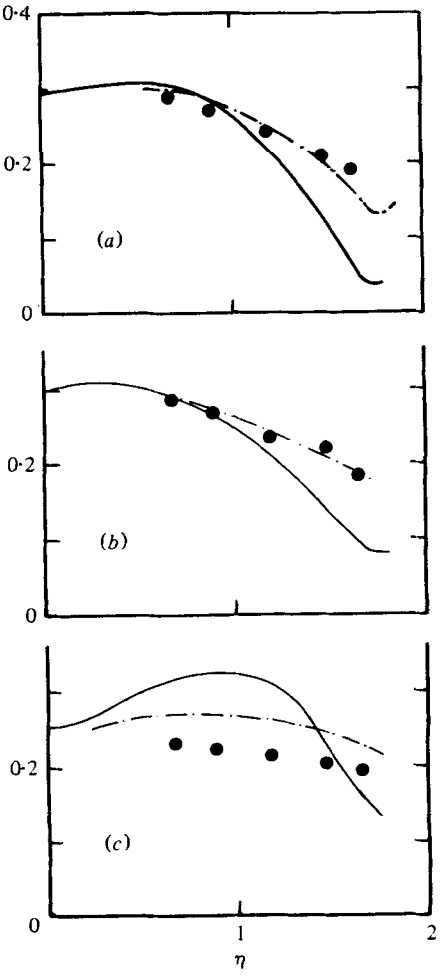

FIGURE 10. R.m.s. velocity and temperature fluctuations across the jet. (a) ●, $u''_{sc}/\overline{U}_0$; ——, $u'/\overline{U}_0$; –·–, $u'_t/\overline{U}_0$. (b) ●, $u''_{sc}/\overline{U}_0$; ——, $v'/\overline{U}_0$; –·–, $v'_t/\overline{U}_0$. (c) ●, $\theta''_{sc}/\overline{\Theta}_0$; ——, $\theta'/\overline{\Theta}_0$; –·–, $\theta'_t/\overline{\Theta}_0$.

$v''_s/\overline{U}_0$ and $\theta''_s/\overline{\Theta}_0$ to be attained. For each η, the asymptotic value attained is different, being smaller for large η. For any given η, this asymptotic state can be taken as a characteristic measure of the r.m.s. of the superposed turbulence.

These characteristic r.m.s. values, denoted by the additional suffix c, are plotted in figures 10(*a*), (*b*) and (*c*) for η = 0·67, 0·89, 1·18, 1·48 and 1·63. For comparison, also shown are the conventional and conditional turbulent r.m.s. values. A partial indication of the accuracy of these characteristic r.m.s. values can be obtained by the scatter in the data of figures 9. A more direct indication comes from figures 11 which show $\langle u_s^2(t)\rangle^{\frac{1}{2}}$, $\langle v_s^2(t)\rangle^{\frac{1}{2}}$ and $\langle \theta_s^2(t)\rangle^{\frac{1}{2}}$ as a function of $t/\overline{T}$ within excursions of $\overline{T}\overline{U}_s/L = 2{\cdot}5$, $\Delta\overline{T}/\overline{T} = \pm 0{\cdot}2$. The data are for η = 0·89. Vertical bars indicate 95% confidence limits. It is interesting to note that, except for the end regions, the r.m.s. quantities are approximately independent of t, so that $x''^2_s \simeq \langle x_s^2(t)\rangle$ for

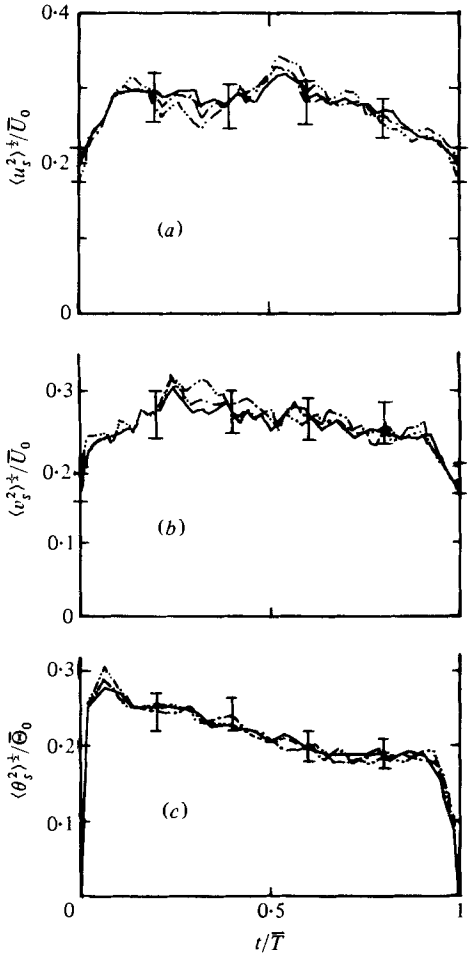

FIGURE 11. R.m.s. velocity and temperature fluctuations about the respective ensemble averages. $\eta = 0{\cdot}89$. ——, $\Delta\overline{T}/\overline{T} = \pm 0{\cdot}28$; –·–, $\pm 0{\cdot}20$; –···–, $\pm 0{\cdot}12$. Vertical bars indicate confidence intervals with 95 % confidence level, $\Delta\overline{T}/\overline{T} = \pm 0{\cdot}20$.

$0{\cdot}1 \leqslant t/\overline{T} \leqslant 0{\cdot}9$. It is also of interest (from figures 10) that $u_s''^2$, $v_s''^2$ and $\theta_s''^2$ are approximately equal to $\overline{(U-\overline{U}_t)_t^2}$, $\overline{(V-\overline{V}_t)_t^2}$ and $\overline{(\Theta-\overline{\Theta}_t)_t^2}$ respectively. This follows from the approximate relation (see (2.4) and (2.3))

$$x_s''^2 = \overline{\overline{\langle (X-\langle X\rangle)^2\rangle}} \simeq \overline{(X-\overline{X}_t)_t^2}.$$

This approximation is not as good for Θ as for U and V because $\overline{\overline{\langle\Theta\rangle}}-\overline{\Theta}_t$ has a non-zero (but small) value for this value of $\overline{T}$.

Figure 12 shows the variation of the ratio u_s''/v_s'' as a function of $\overline{T}$. Again, the ratio is independent of $\overline{T}$ for $\overline{T} \gtrsim L/\overline{U}_a$, and is equal to unity as one would expect for isotropic turbulence. This, in itself, is a significant result, and needs an explanation when one considers that the ratios u'/v' and u_t''/v_t'' are also approximately equal to unity (see table 1). The combination of these two results implies either that the large-scale motion is also not far from being isotropic or that its contribution to the total

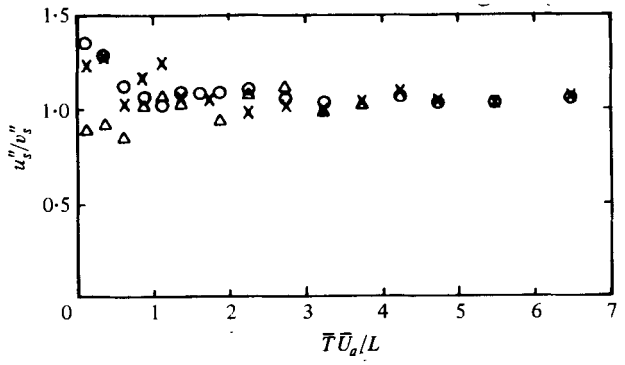

FIGURE 12. Ratio of r.m.s. velocity fluctuations of the superposed turbulence as a function of $\overline{T}$ over which they are defined. ×, $\eta = 0{\cdot}67$; ⊙, $\eta = 0{\cdot}89$; △, $\eta = 1{\cdot}48$.

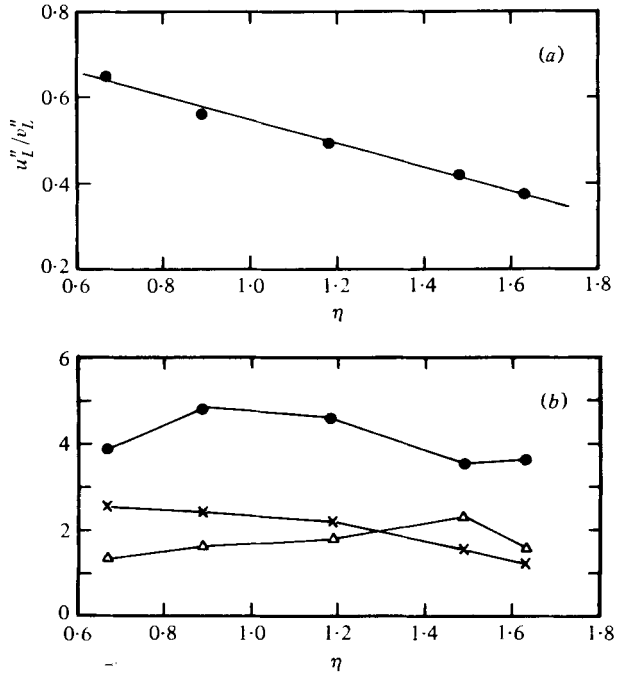

FIGURE 13. (a) Anisotropy of large-scale motion. (b) Ratio of r.m.s. fluctuations of superposed turbulence to those of large-scale patterns. ●, u_s''/u_L''; ×, v_s''/v_L''; △, θ_s''/θ_L''.

mean-square value is not so overwhelmingly large as to influence the degree of anisotropy of the total signal. A measure of anisotropy of the large-scale motion is the ratio u_L''/v_L'' where, for example,

$$u_L'' \equiv \overline{\overline{u_L^2}}^{\frac{1}{2}} = \overline{\overline{[\langle U\rangle - \langle\overline{U}\rangle]^2}}^{\frac{1}{2}}. \tag{4.1}$$

Figure 13(a) shows that this ratio is considerably less than unity, suggesting a high degree of anisotropy. Further, the degree of anisotropy increases almost linearly with increasing η. Figure 13(b) shows that the mean-square contribution of the large-scale motion is generally less than that of the superposed turbulence. This is a fairly small fraction in the case of U (for which $u_s''^2/u_L''^2 \simeq 16$), but is about $\frac{1}{4}$ in the case of V and Θ.

η	$\bar{u}_t/\bar{U}_0$	$\bar{v}_t/\bar{U}_0$	$\bar{\theta}_t/\bar{\Theta}_0$	u'/v'	u'_t/v'_t	$\dot{v}'/\dot{u}'$
0·67	0·006	0·005	0·010	1·07	1·07	1·78
0·89	0·018	0·012	0·037	1·09	1·08	1·77
1·18	0·050	0·033	0·153	1·08	1·05	—
1·48	0·039	0·055	0·270	1·02	0·94	1·80
1·63	0·015	0·048	0·265	0·96	0·90	1·66

TABLE 1. Some turbulence parameters across the jet.

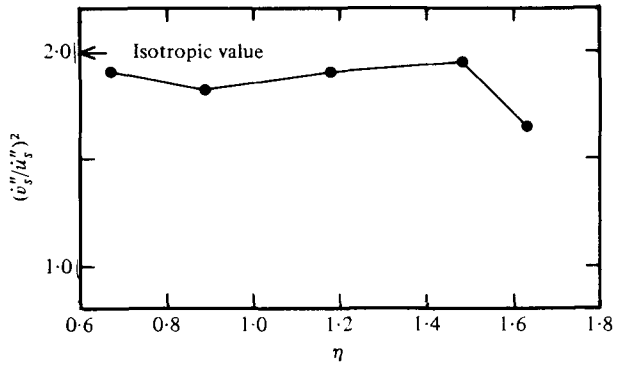

FIGURE 14. Ratio of mean-square derivatives of velocity fluctuations of superposed turbulence.

(*b*) *Mean-square derivatives*

If the superposed motion is locally isotropic, one of the conditions it would have to satisfy is

$$\frac{\overline{\overline{(\partial v_s/\partial t)^2}}}{\overline{\overline{(\partial u_s/\partial t)^2}}} = 2.$$

Using the notation described in § 2.4, we can write this as

$$\dot{v}''^2_s/\dot{u}''^2_s = 2,$$

where a dot indicates a derivative with respect to time. Figure 14 shows that this is approximately satisfied except possibly far away from the axis. As can be seen from table 1, the ratio $\overline{\dot{v}^2}/\overline{\dot{u}^2}$ is not very different from the ratio $\dot{v}''^2_s/\dot{u}''^2_s$, although the latter is probably closer to 2 than the former. This supports our earlier speculation (§ 1) that the contribution of the large-scale motion to the mean-square derivative of a given quantity may be small.† Figure 15 shows that this contribution is about 20 % in the case of θ and about 10 % in the case of v and u. Interestingly, for the ramp model hypothesized by Sreenivasan & Antonia (1977) the ratio of the mean square of the derivative of large-scale motion in Θ to that of the superposed θ fluctuations was estimated by an entirely different (and indirect) method to be about 0·25, consistent with the present more direct estimates.

† The dependence on R_λ of this contribution would need further experimental work.

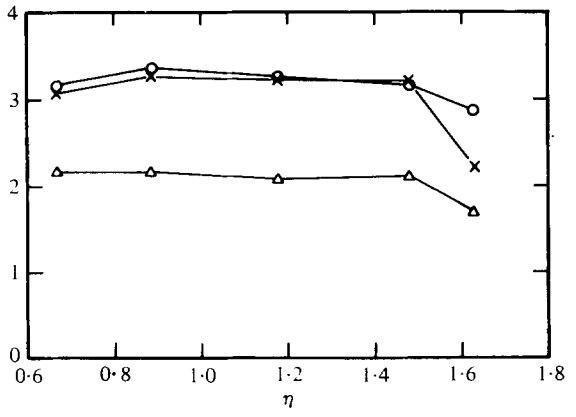

FIGURE 15. Ratio of r.m.s. derivatives of superposed turbulence to those of large scale. ○, $\dot{u}''_s/\dot{u}''_L$; ×, $\dot{v}''_s/\dot{u}''_L$; △, $\dot{\theta}''_s/\dot{\theta}''_L$.

(c) *Turbulent transport by the large scale*

Bradshaw, Ferriss & Johnson (1964) and Bradshaw (1967) suggested that the large-scale motion produces a significant proportion of the shear stress in mixing layers and outer part of a turbulent boundary layer. Lu & Willmarth (1973), on the other hand, showed that a significant fraction of the Reynolds stress in the outer regions of a turbulent boundary layer occurs in scales of motion which are much smaller than the characteristic size of the large eddies. Using simultaneous visual and hot-wire studies, Falco (1977) observed that the largest fluctuations in uv coincided with the occurrence of his typical eddies which have an average size of the order of the Taylor microscale. Using our present technique, it is possible to evaluate the fraction of the average stress or heat flux due to large-scale excursions alone. As the results for the shear stress and heat flux are essentially the same, we shall present data only for the shear stress. Figure 16(*a*) shows the fraction of the contribution to the total shear stress from the large-scale patterns; data correspond to $\overline{T}\overline{U}_a/L = 2{\cdot}5$, $\Delta\overline{T}/\overline{T} = \pm 0{\cdot}2$. It is seen that, in regions of substantial turbulence production, it is the superposed motion that accounts for most of the shear stress. As the distance from the jet axis increases, however, an increasingly larger fraction of the local shear stress arises from the large-scale patterns. (The shear stress itself is small far away from the axis.) We recall that, in the region of significant turbulent energy production, most of the shear stress or heat flux in the large-scale patterns occurs in the 'skin', especially the backs (figures 7 and 8). In this sense, the data of figure 16(*a*) are likely to have overestimated the large-scale contribution in that region.

Some caution is however necessary in interpreting the above result, because of the possible lack of unique correspondence between large-scale structures and large-scale excursions of the same scale: just as some large-scale excursions of a given duration, say $\overline{T}_1$, arise from structures of even larger scale, it is equally possible that some structures of duration $\overline{T}_1$ almost certainly fail to give rise to excursions of duration $\overline{T}_1$. This lack of correspondence is further compounded by the possible multi-valuedness of the turbulent/non-turbulent interface. Even if a spatial array of sensors is used, this question remains essentially unanswered.

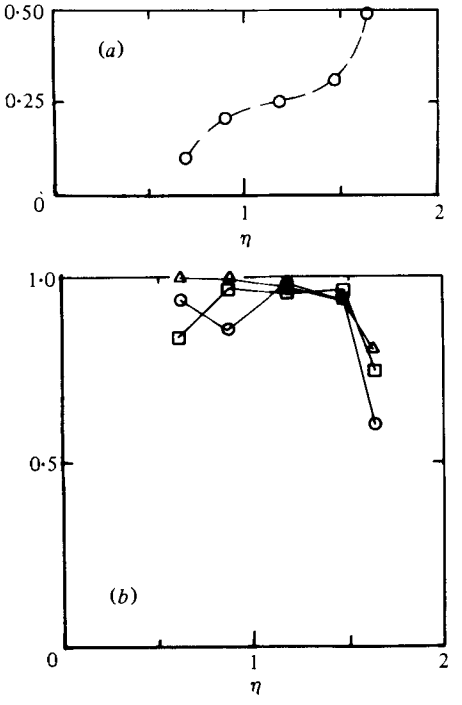

FIGURE 16. (*a*) Fractional contribution of the ensemble averages of large-scale excursions to the local Reynolds shear stress across the jet. (*b*) Correlation coefficients for the ensemble average large-scale excursions. ○, $\overline{\overline{u_L v_L}}/u_L'' v_L''$; □, $\overline{\overline{u_L \theta_L}}/u_L'' \theta_L''$; △, $\overline{\overline{v_L \theta_L}}/v_L'' \theta_L''$.

It was suggested in § 3 that a high degree of correlation exists between ensemble averages of large-scale excursions. We can obtain correlation coefficients for the large-scale motion, defined as

$$C_{xy} = \overline{\overline{x_L y_L}}/x_L'' y_L''$$

These coefficients evaluated for $\overline{T}\overline{U}_a/L = 2{\cdot}5$, $\Delta\overline{T}/\overline{T} = \pm 0{\cdot}2$ are plotted in figure 16(*b*). From the ensemble averages of figures 7(*a*)–(*c*), and the definitions of x_L and x_L'', it is quite clear that the reliability of these correlation values is not very high; simple estimates show that errors of the order of 30 % are quite likely. However, there is little doubt that these results indicate a high degree of correlation within the large-scale motion, except possibly towards the outer edge of the jet.

(*d*) *Probability density functions*

Results of previous sections have emphasized the significant role played by the superposed turbulence. Here, we examine the probability density functions (p.d.f.s) of the superposed motion. Results are presented for $\eta = 1{\cdot}48$ ($\gamma \simeq 0{\cdot}28$). In figure 17, the normalized p.d.f.s of u_s, v_s and θ_s are compared with corresponding conventional and conditional (turbulent) p.d.f.s and Gaussian p.d.f.s (with experimental values of the mean and variance). The differences between the p.d.f.s of u_s, v_s and θ_s from those of u, v and θ or u_t, v_t and θ_t (respectively) are dramatic. It is also clear that the p.d.f.s of u_s, v_s and θ_s are significantly closer to Gaussian form, resembling the situation in homogeneous turbulence, suggesting that the superposed turbulence has a quasi-homogeneous behaviour.

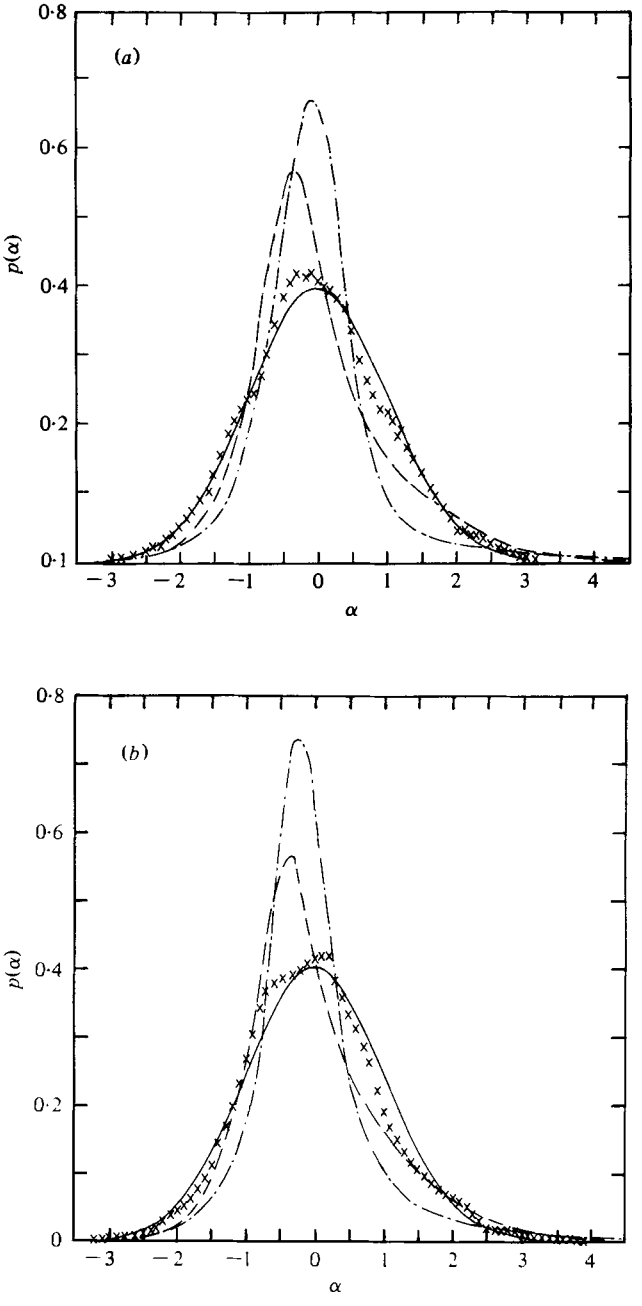

FIGURE 17 (*a*) and (*b*). For legend see p. 765.

Similarly, figure 18 shows p.d.f.s of $\dot{u}_s$, $\dot{v}_s$ and $\dot{\theta}_s$ at $\eta = 1{\cdot}48$. Again, they are compared with corresponding p.d.f.s of conventional derivatives and the Gaussian p.d.f. Although no dramatic differences between $\dot{\theta}$ and $\dot{\theta}_s$ are apparent from this figure, a very significant result concerns the skewness of the derivative of θ_s, as compared with that of θ. To see this clearly, the quantity $\alpha^3 p(\alpha)$ has been plotted against α in

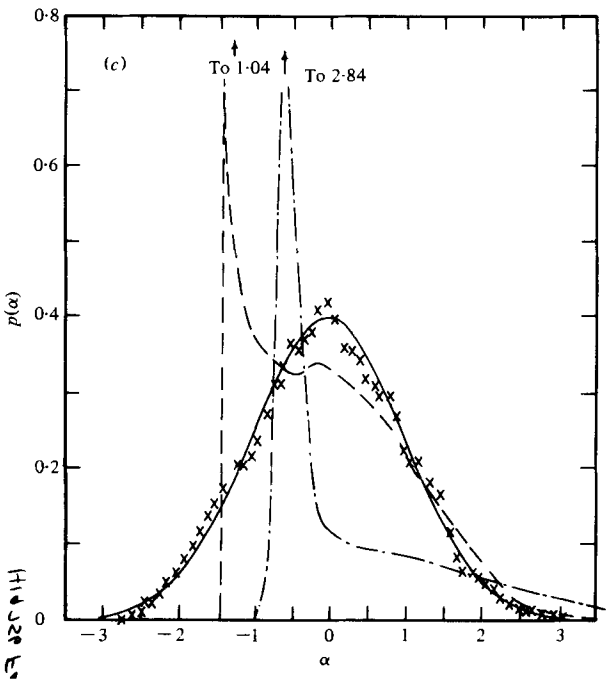

FIGURE 17. Probability density functions. (*a*) ×, $\alpha = u_s/u_s''$; ---, u_t/u_t'; -·-, u/u'; (*b*) ×, $\alpha = v_s/v_s''$; ---, v_t/v_t'; -·-, v/v'; (*c*) ×, $\alpha = \theta_s/\theta_s''$; ---, θ_t/θ_t'; -·-, θ/θ'. For superposed turbulence $\bar{T}\bar{U}_a/L = 2{\cdot}5$, $\Delta\bar{T}/\bar{T} = \pm 0{\cdot}2$. ——, Gaussian.

figure 19, where α is either $\dot{\theta}_s/\dot{\theta}_s''$ or $\dot{\theta}/\dot{\theta}'$. The areas under these curves must be equal to the skewnesses of $\dot{\theta}_s$ and $\dot{\theta}$ respectively. Consistent with all other measurements of temperature derivative found in the literature, the skewness of $\dot{\theta}$ has a magnitude of about 0·87 (as given by the area under full curves). Because of the limited number of samples ($\sim 10^4$), there is considerable scatter in the case of $\dot{\theta}_s$, but it is clear that the skewness of $\dot{\theta}_s$ is much smaller than that of $\dot{\theta}$. It is interesting to note that the most significant changes in $\dot{\theta}_s$ occur in the lobe with $\dot{\theta}_s > 0$, which would indeed be expected if the asymmetric ramp structures are removed from the turbulent signal. Using the dashed line to approximate the points, we obtain $S_{\dot{\theta}_s} \simeq 0{\cdot}33$. We emphasize that the fractional contribution of the superposed turbulence to the *third moment* of $\dot{\theta}$ is considerably smaller, and is about 30 % of that of the total signal.

Because this is an important result, further corroborating evidence would be worthwhile; we can do this by independently evaluating the complementary quantity, namely the contribution of large-scale temperature patterns to the third moment of $\dot{\theta}$. For instance, at $\eta = 0{\cdot}89$, fitting a curve shown in figure 6 to the ensemble average of large-scale excursions, we can show that the contribution of the large scale to the third moment of $\dot{\theta}$ is about 70 %, consistent with our earlier result. (The third moment of the total signal is equal to the sum of contributions from the large-scale and superposed turbulence, if the two scales of motion are independent.) Considering the somewhat limited accuracy of the results plotted in figure 19, and the moderate value of R_λ, a useful conclusion appears to be that the derivative of θ_s has negligible skewness. We conclude that the breakdown of local isotropy is due to the large-scale structure.

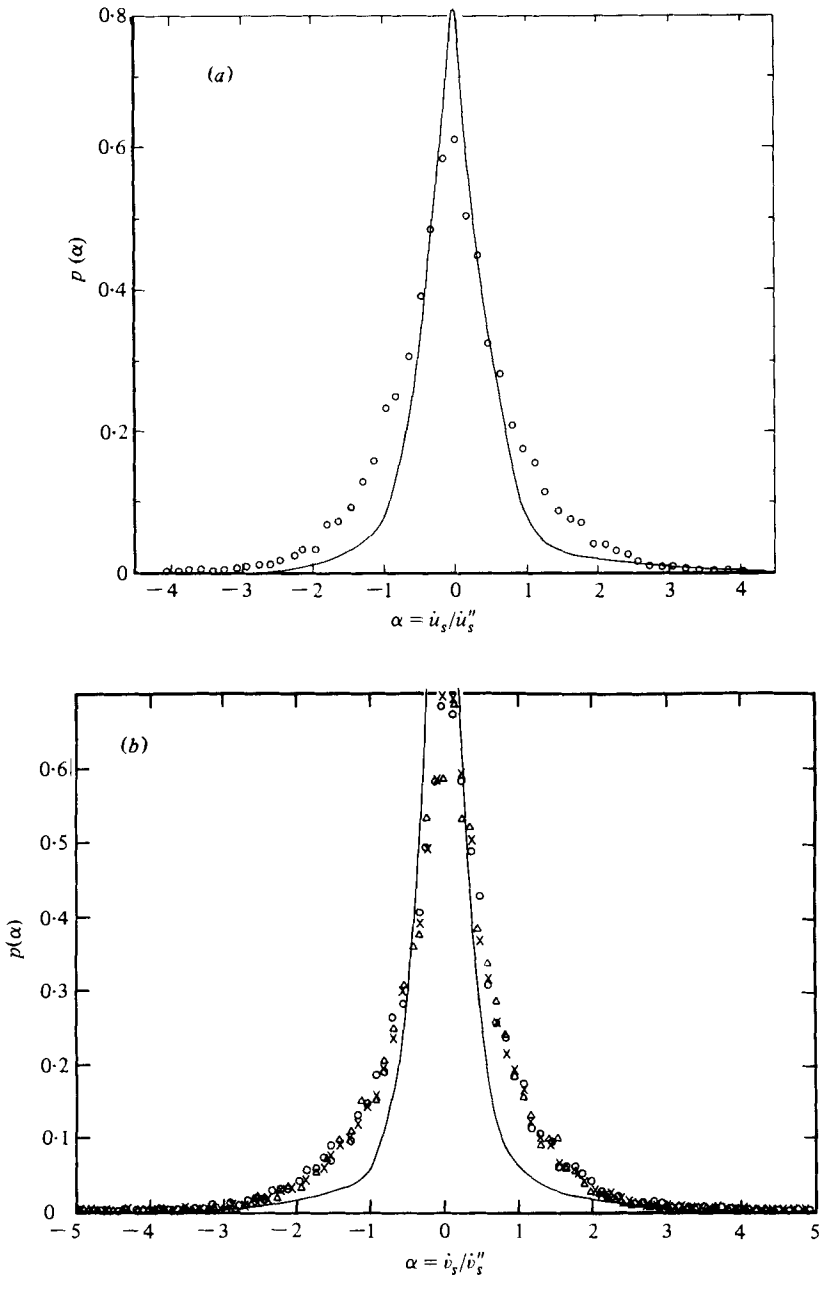

FIGURE 18 (*a*) and (*b*). For legend see p. 767.

(*e*) *Spectral densities of superposed turbulence*

Figure 20(*a*) shows a comparison at $\eta = 0{\cdot}89$ between normalized spectral densities ϕ_u, ϕ_v and ϕ_θ of conventional turbulence quantities and ϕ_{u_s}, ϕ_{v_s} and ϕ_{θ_s} of the superposed fluctuations ($\overline{T}\overline{U}_a/L = 2{\cdot}5$, $\Delta\overline{T}/\overline{T} = \pm 0{\cdot}2$). (Instead of ϕ_u, ϕ_v, ϕ_θ, it would seem more appropriate to use spectral densities of fluctuations in the

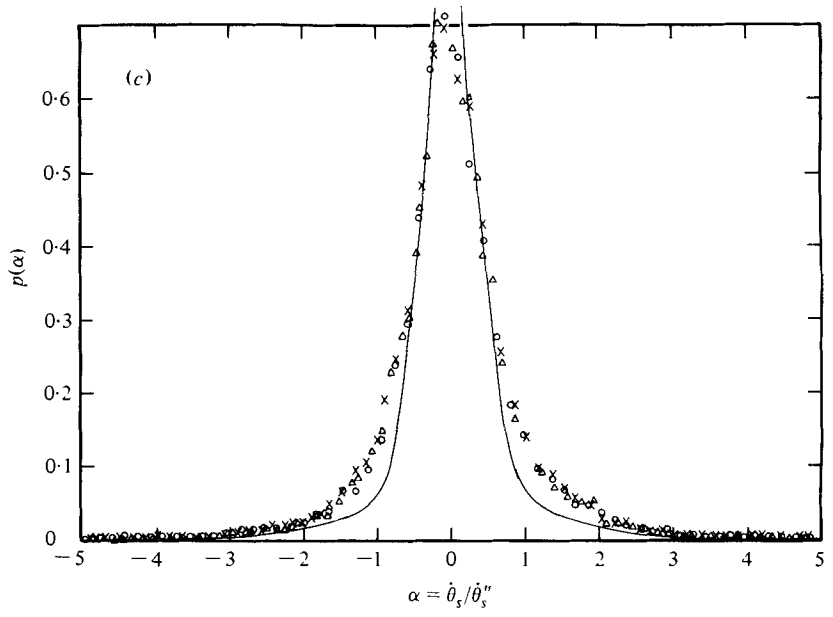

FIGURE 18. Probability density functions of derivatives. (*a*) ○, $\alpha = \dot{u}_s/\dot{u}_s''$; ——, $\dot{u}/\dot{u}'$. (*b*) symbols, $\alpha = \dot{v}_s/\dot{v}_s''$; ——, $\dot{v}/\dot{v}'$. (*c*) symbols, $\alpha = \dot{\theta}_s/\dot{\theta}_s''$; ——, $\dot{\theta}/\dot{\theta}'$. In (*b*) and (*c*) symbols are △, $\Delta\overline{T}/\overline{T} = \pm 0{\cdot}28$; ○, 0·20; ×, 0·12.

turbulent part only of the flow, in order to eliminate the additional effect of intermittency on spectral densities. However, the intermittency factor γ at this station (= 0·93) is almost unity, so that a useful comparison can be made with conventional spectral densities.) The greatest differences between spectra of superposed fluctuations and those of conventional quantities occur in the case of temperature. Because the effect of large-scale motion should no longer be present when we consider the superposed turbulence, we expect all the energy to reside in frequencies $fL/\overline{U}_a \gtrsim 0{\cdot}4$ or $2\pi fL/\overline{U}_a \gtrsim 5$ and none at lower frequencies. However, because of the inherent ambiguities of the one-dimensional spectra in representing the energy of essentially three-dimensional variables (see, e.g., Tennekes & Lumley 1972, p. 248), this last feature is not unambiguously clear from these curves; figure 20(*a*) is not inconsistent with this expectation. Note that all spectra of superposed fluctuations show a mild peak at the low frequency end. Again, the interpretation of these peaks is a little difficult, but one observation is worth making. If f_p is the frequency corresponding to these peaks, the present value of $\overline{U}_1/f_pL$ is in the range 3–4. Allowing for the slightly different normalizing length scale, this is of the same order as the non-dimensional value of the high frequency pulses of Badri Narayanan, Narasimha & Rao (1971) in a turbulent wake, and of Rao, Narasimha & Badri Narayanan (1971) and Ueda & Hinze (1975) in a turbulent boundary layer, and also of the large amplitude small-scale Reynolds stress-carrying motion investigated by Lu & Willmarth (1973) in the outer region of a turbulent boundary layer.

It is instructive to replot the same data without normalizing in both cases, in such a way that the energies at any given frequency are comparable in 'conventional' and superposed turbulence. This can be achieved in the simplest way by suitably

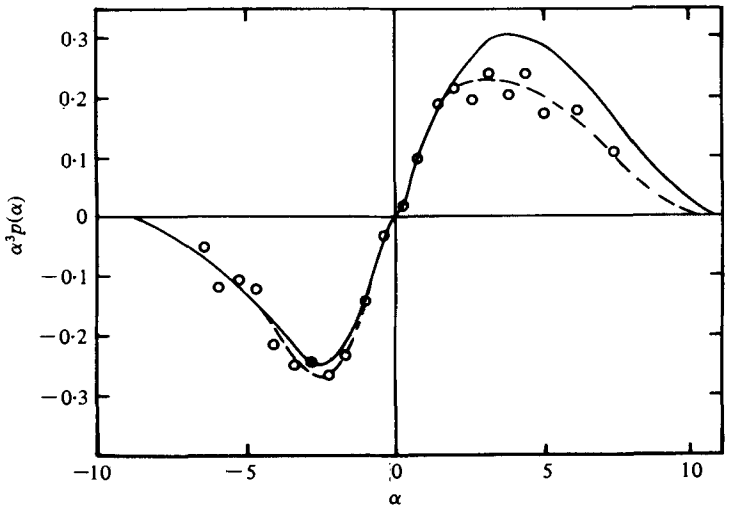

FIGURE 19. The integrand function for the evaluation of skewness of temperature derivatives. $\eta = 1{\cdot}48$. ——, $\alpha = \dot{\theta}/\dot{\theta}'$. ○, $\alpha = \dot{\theta}_s/\dot{\theta}_s''$. ($\overline{T}\overline{U}_a/L = 2{\cdot}5$, $\Delta\overline{T}/\overline{T} = \pm 0{\cdot}2$.) ---, suggested mean through the points.

weighting the spectra of superposed fluctuations, e.g. multiplying ϕ_{θ_s} by the ratio $\overline{\overline{\theta_s^2}}/\overline{\theta^2}$. We denote these weighted spectra by ψ_{u_s}, ψ_{v_s} and ψ_{θ_s}, corresponding to u_s, v_s and θ_s respectively. Figure 20(*b*) shows a comparison between ψ_{u_s}, ψ_{v_s} and ψ_{θ_s} and ϕ_u, ϕ_v and ϕ_θ. It is immediately clear that differences between the superposed turbulence and the conventional turbulence occur essentially at lower frequencies, and that there are only very minor differences at high frequencies. The significance of this result will be discussed in § 5.

To ascertain the accuracy of the present spectral information related to the superposed motion, the following check was performed. By using the technique described in § 2.4, in addition to the spectra of u_s, v_s and θ_s corresponding to $\overline{T}\overline{U}_a/L = 2{\cdot}5$, $\Delta\overline{T}/\overline{T} = \pm 0{\cdot}2$, spectra of the fluctuations u, v and θ, also from the same excursions, were obtained. By appropriately weighting these spectral densities and forming the required differences, spectral densities of the ensemble average shapes may be obtained. The latter information can also be obtained by fitting simple algebraic expressions to the ensemble average shapes of figure 7, and subsequently doing a Fourier analysis. For all cases examined where both sets of calculations were performed, the agreement was found to be quite satisfactory.

5. Conclusions and further discussion

The main conclusions that emerge are:

(*a*) Some identifiable patterns can be found in velocity and (especially) temperature signals.

(*b*) The patterns contain certain highly correlated non-trivial mean shapes which can be determined by a selective ensemble averaging procedure outlined in § 2.4. The fraction of the turbulent energy associated with these patterns is small throughout the flow. The corresponding fraction of the turbulent shear stress or heat flux is

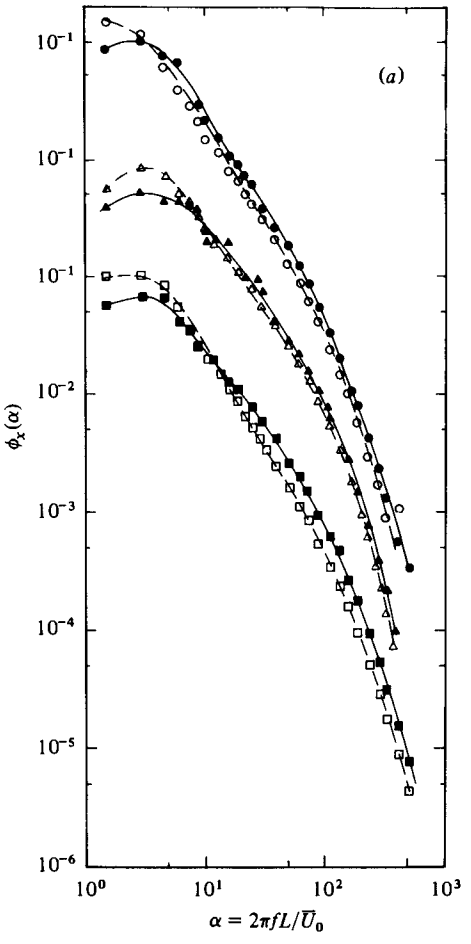

FIGURE 20 (*a*). For legend see p. 770.

also small in the region of turbulent energy production, but becomes somewhat larger in the outer regions of the jet.

(*c*) In the case of v and θ, mean shapes of these patterns are highly asymmetric, and account for most of the skewness of the respective derivatives.

(*d*) After removal of these mean patterns from the respective signals, statistics of the remainder called the 'superposed' turbulence, are consistent with local isotropy. In particular, the derivative of the superposed fluctuation θ_s has negligible skewness in comparison with the derivative of θ.

(*e*) The superposed motion carries a significant proportion of turbulent stresses (both normal and shear), especially in the region of large turbulence production.

(*f*) The probability density functions of the superposed fluctuations are nearly Gaussian in shape.

(*g*) Their spectra reveal a mild peak at a non-dimensional frequency comparable to the bursting frequency observed in various shear flows.

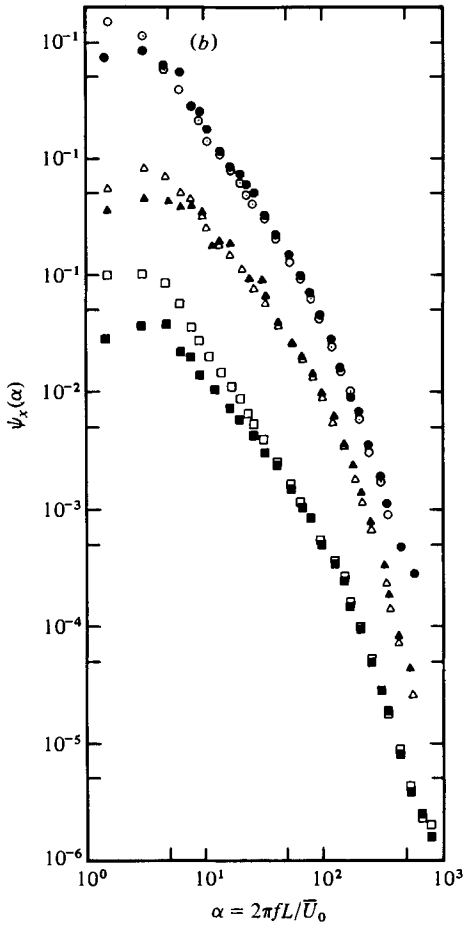

FIGURE 20. (*a*) Normalized power spectral densities ϕ_x of conventional turbulent and superposed fluctuations. $\eta = 0{\cdot}89$. ○, $x = u$; ●, u_s. △, $x = v$; ▲, v_s. □, $x = \theta$; ■, θ_s. Full lines through filled symbols and broken lines through open symbols are drawn only for clarity. (*b*) Weighted spectra ψ_x of the superposed turbulence compared with the spectra of conventional turbulence quantities. Open symbols refer to conventional quantities and filled-in symbols to the superposed motion. ○, u; △, v; □, θ. $\eta = 0{\cdot}89$.

When interpreting these results in the context of the detailed flow structure, it is necessary to remember the limitation of single-point measurements in obtaining information about three-dimensional structures. Despite this limitation, it is reasonably clear that large-scale patterns or excursions in turbulent signals arise when large-scale structures cross the measuring probe. Conclusion (*b*) above then means that the turbulent motion that rides over the large turbulent structures carries a significant part of the Reynolds shear stress. This is not necessarily in conflict with the one-dimensional spectral measurements of uv, which show that a large part of $\overline{uv}$ occurs at low frequencies. The intermittency of uv may spuriously lead to this latter result. Further, the characteristic scale of the superposed fluctuations is not small in that it is much larger than that of the dissipative scales of

turbulence. Unfortunately, it is not possible, at present, to identify this scale with the other more familiar scales of turbulence.

With regard to the applicability of local isotropy, a significant result is that the presence of anisotropic large-scale structures is responsible for the observed skewness of θ_x. Gibson *et al.* (1977) also considered this possibility, but concluded that ramp-like structures can in fact produce a much larger value of skewness than observed, presumably due to the specific model they chose for the superposed small-scale motion. Another implication of Gibson *et al.* is that the presence of mean shear and mean temperature gradient is sufficient to produce large-scale ramp-like structures which, we now believe, are responsible for the breakdown of local isotropy. In support of this implication we recall that Antonia *et al.* (1978) and Sreenivasan *et al.* (1979) have shown that for heated grid turbulence (where temperature fluctuations reveal no ramp-like structures) the skewness of $\theta_x \simeq 0$. The data of figure 1, which encompass measurements in various shear flows, suggest that the magnitude of S_{θ_x} is insensitive to the (suitably defined non-dimensional) magnitude of the shear. It thus seems that the breakdown of local isotropy is connected to the presence of mean shear in a somewhat subtle way†: only its presence and sign are important and not its magnitude!

To clarify this and other issues, further work is clearly desirable in different flows and preferably at high Reynolds numbers. Although all measurements reported here were made at a moderate R_λ, this does not appear to be a crucial factor, as the following argument would suggest. With the present classification in mind, it is convenient to regard the skewness S_{θ_x} as being made up of separate contributions from the large and small scales of θ, with no significant interaction between them. At small Reynolds numbers, the small-scale θ is also likely to be locally anisotropic (and hence its derivative skewed). As the Reynolds number increases, the small scale becomes more closely isotropic, so that there is a tendency for S_{θ_x} to decrease initially with increasing R_λ. For Reynolds numbers which are large, the small scale contributes little to the skewness of θ_x, and the large scale is solely responsible for it; hence the observed independence of S_{θ_x} on R_λ. From figure 1, it appears that $R_\lambda \gtrsim 50$ can be considered 'sufficiently large' in this respect. It is plausible that with increasing R_λ the fractional contribution of the large scale to the mean-square derivative may decrease and become negligibly small in the limit of infinitely large R_λ, but as long as the large-scale patterns have sharp asymmetric edges, there will be a contribution to S_{θ_x} from the large scale.

An implication of these results is that, in some sense, a small fraction of high frequency content is due to the large scale. These high frequencies which contribute to the skewness of θ_x may or may not overlap, in general, with the dissipative range of frequencies, depending on the Reynolds number and the way in which the sharp edges of large-scale excursions vary (if they do) with R_λ. Simple estimates of the skewness-contributing frequencies can be made for the present flow. At $\eta = 0{\cdot}89$, for example, the skewness of θ_x arises from excursions essentially in the range of duration $1 \lesssim \overline{T}\overline{U}_a/L \lesssim 20$. While there are very few or no excursions of larger duration, smaller excursions are symmetric on average (see figure 6) and hence do not contribute to S_{θ_x}. Noting that the ratio of the sharply rising part to that of the

† More is now known about the role of mean shear and mean temperature gradient in producing the skewness of θ_x (Sreenivasan & Tavoularis, in preparation).

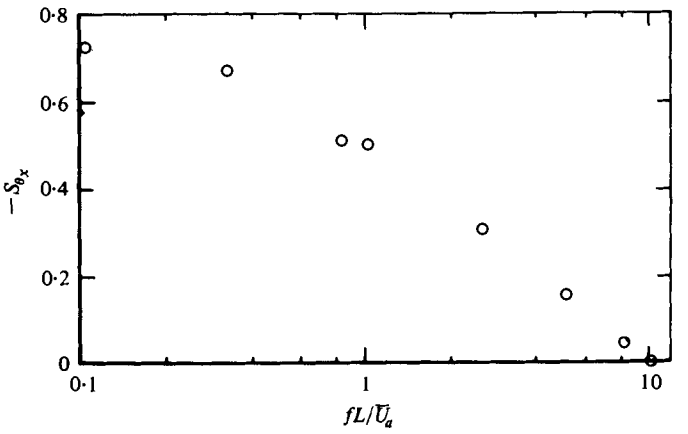

FIGURE 21. Variation of skewness of θ_x with high-pass cut-off frequency, $\eta = 0$.

gradually sloping part of $\langle\Theta\rangle$ (i.e. the ratio AB/BC in figure 6) to be about 1/20, most of the skewness can be considered to arise from the frequency range $1 \lesssim fL/\overline{U}_a \lesssim 20$. This is also the range of frequencies with significant dissipation, at least with respect to the θ_x spectrum, which peaks at $fL/\overline{U}_a \simeq 6$. It is thus clear that the skewness-contributing frequencies cannot be separated from those contributing to $\overline{\theta_x^2}$. Consequently, in the range $1 \lesssim fL/\overline{U}_a \lesssim 20$, some consistent differences must be observed between the θ spectra (which contain all frequencies) and θ_s spectra (which contain no skewness-contributing-high frequencies). But because the skewness-contributing frequencies make only a small contribution to the mean-square value of θ_x, these differences cannot be expected to be dramatic, as is in fact shown by figure 20(*b*).

These arguments suggest a simple experiment. If we pass θ through a band-pass filter with the low pass setting at the Kolmogorov frequency and with a variable high pass setting, and compute the skewness of the derivative of the filter output, the following result should occur. As the high pass setting varies from zero to $fL/\overline{U}_a \simeq 1$, little change should take place in the skewness of the derivative of band-pass θ. However, as the high pass setting moves through the range $1 \lesssim fL/\overline{U}_a \lesssim 20$, the skewness must gradually decrease and must vanish for $fL/\overline{U}_a \approx 20$. The result of such an experiment (for θ at $\eta = 0$) is shown in figure 21. Considering the simplified nature of these arguments and the fact that analogue instrumentation was used in this set of measurements, the figure lends overall support to our arguments. Recently, Tavoularis (1978) has also obtained similar results using digital techniques in a uniformly sheared flow with a constant mean temperature gradient.

K. R. Sreenivasan is indebted to Professor W. H. Schwarz and Mr S. Morris for their useful comments on an earlier draft of this paper, and to Professor S. Corrsin for his encouragement and generously making available the financial support from U.S. National Science Foundation, Atmospheric Science Division, Grant no. P41-4068, during the final phases of this work.

The authors are grateful to Professor R. W. Bilger for the use of his jet facility. The support of the Australian Research Grants Committee is gratefully acknowledged.

Flow	R_λ	$(\epsilon/\nu)^{\frac{1}{2}}\lvert\partial\overline{U}/\partial y\rvert^{-1}$	$k_\eta/10k_p$	$S_{\theta x}$
Heated jet				
$\eta = 0{\cdot}89$	220	23	16	$-0{\cdot}90$
$\eta = 1{\cdot}48$	125	17	16	$-0{\cdot}88$
Heated boundary layer (Mestayer *et al.* 1976)	750	66	82	$+0{\cdot}85$

TABLE 2. Conventional tests for local isotropy.

Appendix A. General criteria for local isotropy in the jet

The necessary basis for a quantitative assessment of local isotropy has been suggested by Corrsin (1957, 1958). We shall here consider two of the criteria discussed by Corrsin. His arguments are essentially that the necessary condition for local isotropy to be a good approximation at a given wavenumber is that the time scale characterizing the transfer of energy to higher wavenumbers must be small compared with, say, the inverse of mean rate of strain. He showed that, in the range of wavenumbers where inertial transfer and viscous dissipation ϵ are both important, the condition is

$$(\epsilon/\nu)^{\frac{1}{2}} \gg |\partial\overline{U}/\partial y|.$$

Another requirement is that the wavenumbers be higher than those corresponding to the turbulent energy production. Corrsin (1958) estimated this latter wavenumber k_p to be

$$k_p \approx \frac{1}{v'}\left|\frac{\partial\overline{U}}{\partial y}\right|.$$

For the dissipative part of the spectrum to be governed by isotropic conditions, all wavenumbers over which significant dissipation occurs should be greater than k_p. If the wavenumber k_d corresponding to the peak of the dissipation spectrum is taken as a representative measure of the dissipative wavenumbers, we require then that $k_d \gg k_p$. Noting that usually $k_d \approx 0{\cdot}1k_\eta$ (see, e.g., the summary diagram of Grant, Stewart & Moilliet 1962), where k_η is the Kolmogorov wavenumber, we should have

$$k_\eta \gg 10k_p.$$

Table 2 lists the Reynolds number, the ratios $(\epsilon/\nu)^{\frac{1}{2}}\lvert\partial\overline{U}/\partial y\rvert^{-1}$ and $k_\eta/10k_p$ at two radial positions $\eta = 0{\cdot}89$ and $1{\cdot}48$ in the present jet flow. For comparison, corresponding data are provided for a fairly high Reynolds experiment (Mestayer *et al.* 1976) in a heated turbulent boundary layer. It is clear from these considerations that local isotropy would be expected to prevail over most of the dissipative scales of motion.

Appendix B. Experiments with random noise

It is necessary to establish that ensemble averaging and other signal-processing techniques used in this paper do not artificially produce 'patterns' where none exist. In this appendix, we report on the result obtained from applying the ensemble averaging technique to random white and 'patternless' noise produced by a commercial random noise generator. A threshold was selected, as in the case of turbulent

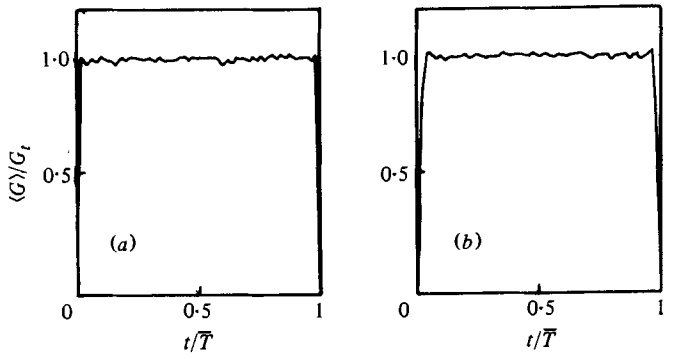

FIGURE 22. Ensemble averages for random white noise. (*a*) $\bar{T}$ = 150 sampling intervals. (*b*) $\bar{T}$ = 50 sampling intervals. $\Delta\bar{T}/\bar{T} = \pm 0{\cdot}20$.

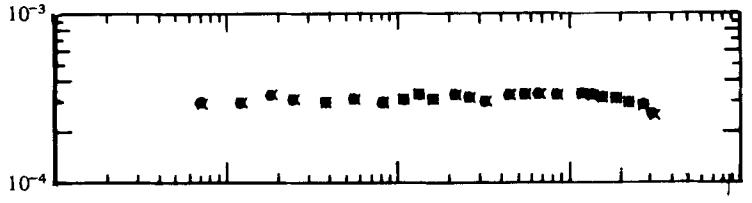

FIGURE 23. Spectral densities of random white noise. ●, total noise signal. ×, 'superposed' fraction of noise.

signals, but with the difference that, for the random noise signal, no real meaning can be attached to the threshold. All excursions within a given range of duration were ensemble averaged and the results are shown in figure 22 for two values of $\bar{T}$. Results corresponding to other durations are essentially similar and exhibit only minor and unimportant differences from those shown in the figure. Over the entire duration of the excursions, the amplitude of ensemble averages is uniform, suggesting that the shapes shown in figures 7 and 8 are not a spurious result of the technique but genuine features of turbulence signals. Further, in the case of random noise, the amplitude (which is independent of $\bar{T}$) is exactly equal to the time mean of the noise above the threshold, i.e. the time mean value of all (pseudo-) excursions forming the ensemble. If $\langle G\rangle$ and $\bar{G}_t$ represent respectively the ensemble average shape of pseudo-excursions of a given duration and the time mean value of the random noise above the threshold, we have, in the notation of § 2.4,

$$\langle\overline{\overline{G}}\rangle \simeq \bar{G}_t \simeq \langle G\rangle$$

for all $\bar{T}$. This suggests that one way of emphasizing the structure in ensemble average shapes for a turbulent signal x is to plot the quantity $\langle x\rangle - \bar{x}_t = \langle x - \bar{x}_t\rangle$. If such plots reveal a characteristic shape whose amplitude is substantially different from zero, it is likely that this shape identifies some definite non-trivial structure.

For relatively low frequencies significant differences are observed between the spectral density of a turbulence signal x and that of its small-scale fraction x_s (figures 19*a*, *b*). Computations of the analogous spectral densities for white noise are

shown in figure 23. It is clear that the 'superposed' random noise has precisely the same spectral density as the total random noise. The differences between ϕ_x and ϕ_{x_s} in figures 19(*a*) and (*b*) must arise from genuine features of turbulence signals.

REFERENCES

ANTONIA, R. A. & VAN ATTA, C. W. 1975 *J. Fluid Mech.* **67**, 273.

ANTONIA, R. A. & ATKINSON, J. D. 1976 *Phys. Fluids* **19**, 1273.

ANTONIA, R. A., PRABHU, A. & STEPHENSON, S. E. 1975 *J. Fluid Mech.* **72**, 455.

ANTONIA, R. A., CHAMBERS, A. J., VAN ATTA, C. W., FRIEHE, C. A. & HELLAND, K. N. 1978 *Phys. Fluids* **21**, 509.

BADRI NARAYANAN, M. A., NARASIMHA, R. & RAO, K. N. 1971 *Proc. 4th Australasian Conf. on Hydraulics and Fluid Mech.*, Monash University, p. 73.

BRADSHAW, P. 1967 *J. Fluid Mech.* **29**, 625.

BRADSHAW, P., FERRISS, D. H. & JOHNSON, R. F. 1964 *J. Fluid Mech.* **19**, 591.

CORRSIN, S. 1949 *J. Aero. Sci.* **16**, 757.

CORRSIN, S. 1957 *Symp. on Naval Hydrodyn.* (ed. F. S. Sherman), p. 373.

CORRSIN, S. 1958 *N.A.C.A. R. & M.* 58B11.

FALCO, R. E. 1977 *Phys. Fluids* **20**, S124.

FREYMUTH, P. 1978 *Phys. Fluids* **21**, 2114.

FREYMUTH, P. & UBEROI, M. S. 1971 *Phys. Fluids* **14**, 2574.

FREYMUTH, P. & UBEROI, M. S. 1973 *Phys. Fluids* **16**, 161.

GIBSON, C. H., STEGEN, G. R. & WILLIAMS, R. B. 1970 *J. Fluid Mech.* **41**, 153.

GIBSON, C. H., FRIEHE, C. A. & MCCONNELL, S. O. 1977 *Phys. Fluids* **20**, S156.

GRANT, H. L., STEWART, R. W. & MOILLIET, A. 1962 *J. Fluid Mech.* **12**, 241.

JENKINS, P. E. & GOLDSCHMIDT, V. W. 1976 *Phys. Fluids* **19**, 613.

LARUE, J. C. & LIBBY, P. A. 1976 *Phys. Fluids* **19**, 1864.

LU, S. S. & WILLMARTH, W. W. 1973 *J. Fluid Mech.* **60**, 481.

MESTAYER, P. G., GIBSON, C. H., COANTIC, M. F. & PATEL, A. S. 1976 *Phys. Fluids* **19**, 1279.

RAO, K. N., NARASIMHA, R. & BADRI NARAYANAN, M. A. 1971 *J. Fluid Mech.* **48**, 339.

SREENIVASAN, K. R. & ANTONIA, R. A. 1977 *Phys. Fluids* **20**, 1986.

SREENIVASAN, K. R. & ANTONIA, R. A. 1978 *A.I.A.A. J.* **16**, 867.

SREENIVASAN, K. R., ANTONIA, R. A. & BRITZ, D. 1978 Local isotropy and large structures in a heated turbulent jet. *Dept. of Mech. Engng Tech. Note* FM 27, Univ. of Newcastle, Australia.

SREENIVASAN, K. R., ANTONIA, R. A. & DANH, H. Q. 1977 *Phys. Fluids* **20**, 1238.

SREENIVASAN, K. R., TAVOULARIS, S., HENRY, R. & CORRSIN, S. 1979 Submitted to *J. Fluid Mech.*

SUNYACH, M. & MATHIEU, J. 1969 *Int. J. Heat Mass Transfer* **12**, 1679.

TAVOULARIS, S. 1978 Experiments in turbulent transport and mixing. Ph.D. Thesis, The Johns Hopkins University, Baltimore.

TENNEKES, H. & LUMLEY, J. L. 1972 *A First Course in Turbulence*. Cambridge, Massachusetts: The M.I.T. Press.

TOWNSEND, A. A. 1948 *Aust. J. Scientific Res.* A **1**, 161.

TOWNSEND, A. A. 1976 *The Structure of Turbulent Shear Flow*. Cambridge University Press.

UEDA, H. & HINZE, J. O. 1975 *J. Fluid Mech.* **67**, 125.

WYNGAARD, J. C. 1971 *J. Fluid Mech.* **48**, 763.